43rd AIAA Aerospace Sciences Meeting, 10–13 January 2005, Reno, NV

Direct numerical simulation of passive scalar mixing in spatially evolving turbulent round jets

Pradeep Babu* & Krishnan Mahesh†

Aerospace Engineering and Mechanics

University of Minnesota

Direct numerical simulation of passive scalar transport in a spatially evolving turbulent jet is performed at Reynolds number of 2400 and Schmidt number of unity. The computational domain extends upstream of the jet exit plane to allow for entrainment near the exit plane. Good comparison with experimental data is obtained for the mean velocity, mean scalar concentration, and fluctuations of velocity and scalar. The instantaneous radial profiles of velocity and passive scalar are examined. The velocity and scalar profiles are shown to be qualitatively similar, and alternate between 'top–hat' and 'triangle' shapes. The profiles are found to be determined by entrainment from the free–stream into the jet and this behavior yields a Gaussian mean. The role of diffusion in scalar transport is studied for its relevance to mixing transition. The instantaneous convective and diffusive terms in the passive scalar transport equation are analyzed, and diffusion–dominated regions are identified. Diffusion–dominated regions occur in very thin regions closer to the jet center. However, diffusion is important over fairly thick, 'brush–like' regions near the jet edge. Higher residence times near the jet edge are thought responsible for this behavior. It is speculated that these brush–like regions determine the overall effect of Reynolds number on the scalar fluctuations. The width of these outer regions is expected to decrease with increase in Reynolds number, and the scalar fluctuations are hypothesized to undergo mixing transition once these outer regions are thin compared to the jet diameter.

I. Introduction

A round jet issuing from an orifice into quiescent air is a classical free shear flow problem which has been studied by many researchers. Early experimental work includes Corrsin (1943), Corrsin & Uberoi (1950, 1951) and Wygnanski & Fiedler (1969). Corrsin & Uberoi (1950) used hot–wire measurements to measure temperature fluctuations in turbulent jets. Wygnanski & Fiedler (1969) performed hot–wire measurements to study turbulence intermittency, skewness, correlations and mean velocity. Their study also examined Taylor's hypothesis and the existence of different convection velocities for different scales of motion. Recent experiments on round jets that provide data on mean velocities, turbulent intensities, stresses, and scalar statistics include Panchapakesan & Lumley (1993), Hussein et al (1994) and Dowling & Dimotakis (1990). Self–similarity in turbulent jets has been of interest for the past few decades. The experiments of Wygnanski & Fiedler (1969), Panchapakesan & Lumley (1993) and Hussein et al (1994) conclude that jets attain universal self–similar profiles about 15 jet exit diameters after the potential core closes. George (1989, 1990) suggests that the governing equations allow similarity solutions which are dependent on factors like initial conditions and domain geometry.

An important application of turbulent jets is the mixing of scalars, both active and passive. Note that a passive scalar does not affect the turbulent velocity field while an active scalar affects the velocity field, generally due to chemical reactions. A review of passive scalar mixing properties in turbulent flow which include spectra, probability density functions and variance is performed by Warhaft (2000). Similar to the

*Graduate Research Assistant, AIAA student member

†Assistant Professor, AIAA member

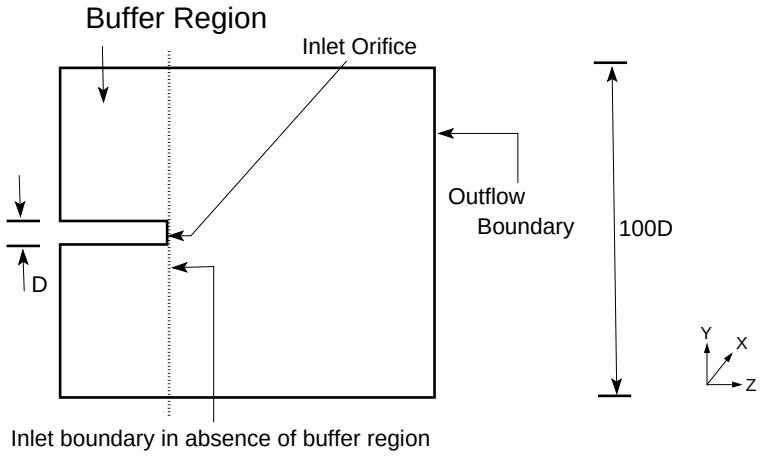

Figure 1. Schematic of the computational domain. A radial cross–section is shown.

velocity fields, there have been numerous studies on the self–similarity of a passive scalar, e.g. Becker et al (1967), Birch et al (1978), Lockwood & Moneib (1980), Dahm & Dimotakis (1985), Dowling & Dimotakis (1990), and Lubbers et al (2001). Oboukhov (1949), Corrsin (1951), Batchelor et al (1959) and others have shown that turbulent scalar field statistics and turbulent velocity field statistics at small scales are similar if the scalar diffusivity and kinematic viscosity are of comparable magnitude. At high Reynolds numbers, the statistics of velocity field and scalar differ appreciably. Dowling & Dimotakis (1990) performed scalar measurements using Rayleigh scattering in turbulent jets. They suggest that self–similarity of mean velocity and concentration depends only on Reynolds number, while self–similarity of the scalar fluctuations also depend on the Schmidt number. The self–similar mean scalar profile is observed to be Gaussian by many experimentalists, e.g. Corrsin & Uberoi (1950), Becker et al (1967), Birch et al (1978), Lockwood & Moneib (1980), Dahm (1985) and Dowling & Dimotakis (1990). Schefer et al (1994) investigated the instantaneous velocity and scalar profiles in a non–reacting CH_4 jet. They found that these instantaneous profiles vary considerably from the mean Gaussian exhibited by the mean velocity and scalar concentration. Similar behavior can be observed in experimental data of Dahm & Dimotakis (1987) in water jets and van Cruyningen et al (1990) in air jets.

Many scalar mixing models have been suggested over the years. Broadwell & Mungal (1991) reviewed few mixing models and found good agreement between experiments and mixing models proposed by Broadwell & Breidenthal (1982) and Kerstein (1990). Broadwell & Breidenthal (1982) suggest a mixing model based on flamelets and Kolmogorov cascade leading to scales where molecular mixing and chemical reaction occur. Kerstein (1990) proposes a linear–eddy model for two unmixed species by simulating the time development along a co–moving transverse line. It is based on the assumption that scalar evolves by molecular diffusion and turbulent convection modeled by randomly occurring spatial rearrangements. Broadwell & Mungal (1991) suggest that the mixing model by Broadwell & Breidenthal (1982) should enable studies on jet flame blowout while the mixing model by Kerstein (1990) should treat the effects of Reynolds, Schmidt and Damköler numbers.

There has been considerable work on the nature of scalar interfaces and scalar dissipation. Prasad & Sreenivasan (1990) studied the temporal intermittency of turbulent flows and qualitative propagation speeds of the scalar interface. Joint statistics of concentration fluctuation, fluctuations gradients and its dissipations were obtained. More recently, Su & Clemens (2003) have performed experiments in gas–phase planar turbulent jets. They examine the magnitude of dissipation length scales of turbulent mixing and also the dependence of that scale on the flow outer–scale Reynolds number. They find that Taylor scaling does not play a significant role in the scalar dissipation process. Pantano et al (2003) performed direct numerical simulations in turbulent planar shear layer with and without heat release. They study the probability density functions of scalar and conditional rate of scalar dissipation to show that reaction rate decreases substantially with heat release.

The present work uses direct numerical simulation to study some important mixing characteristics of passive scalars in spatially evolving turbulent round jets. The paper is organized as follows. Section II

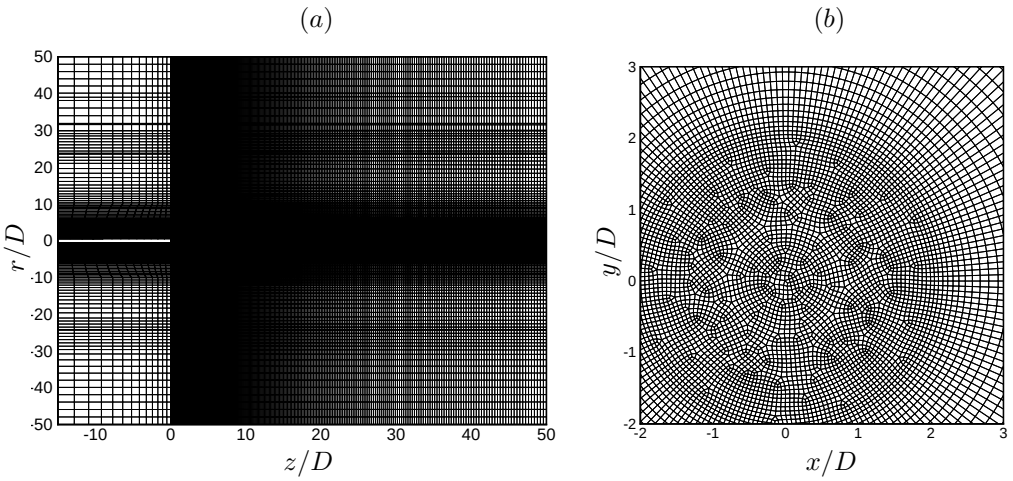

Figure 2. Cross–sections of the grid (*a*): Radial cross–section of the grid (*b*): Axial cross–section of the grid close to the jet centerline. Note the unstructured hexahedral elements close to the jet center.

describes details of the simulation, including results of convergence studies. Sections III(A) and III(B) show that the simulation results agree well with experimental data. Instantaneous profiles of the velocity and scalar fields are examined in section IV(A). Dependence on entrainment from free–stream into jet is shown. Section IV(B) analyzes scalar budgets of convection and diffusion and examines the importance of viscous diffusion in the mixing process. The results are used to speculate on the nature of mixing transition. Section V concludes the paper.

II. Simulation details

The governing equations are the incompressible Navier–Stokes equations (equations 1–2) and the passive scalar transport equation (equation 3)

$$\frac{\partial u_i}{\partial x_i} = 0, \tag{1}$$

$$\frac{\partial u_i}{\partial t} + \frac{\partial (u_i u_j)}{\partial x_j} = \frac{\partial p}{\partial x_i} + \frac{1}{Re}\frac{\partial^2 u_i}{\partial x_j \partial x_j}, \text{ and} \tag{2}$$

$$\frac{\partial c}{\partial t} + \frac{\partial (c u_i)}{\partial x_j} = \frac{1}{Re\ Sc}\ \frac{\partial^2 c}{\partial x_j \partial x_j}, \tag{3}$$

where Re is the Reynolds number of the jet based on the jet exit diameter and the bulk velocity, and Sc denotes the Schmidt number of the passive scalar defined as the ratio of kinematic viscosity to the molecular diffusivity. The variables, u_i, p, and c denote the non–dimensional velocity, pressure and passive scalar concentration. The reference velocity is the bulk velocity at the jet exit and the reference scalar concentration is the concentration of passive scalar at jet exit.

The numerical algorithm is described in detail by Mahesh et al. (2004) and will only be summarized here. The algorithm is a predictor–corrector formulation that emphasizes discrete energy conservation for the convection and pressure terms on unstructured grids with arbitrary elements. The Cartesian components of velocity and pressure are stored at the centroids of the grid elements, and face–normal velocities are stored at the centroids of the faces. The nonlinear and viscous terms are used to obtain a predictor value for the cell–centered velocities. The predicted values of u_i are used to obtain predicted values for the face–normal velocities, which are then projected to obtain the pressure. Once the pressure is obtained, the Cartesian velocities are updated using a least–squares formulation for the pressure gradient. Time advancement is explicit and uses the second–order Adams Bashforth method. The algorithm has been validated for a variety of turbulent flows by Mahesh et al. (2004), and shown to be non–dissipative yet robust, at high Reynolds numbers in very complex geometries.

A schematic of the computational domain is shown in figure 1. The computations used unstructured grid of hexahedral elements. Note that the computational domain extends upstream of the jet exit to allow

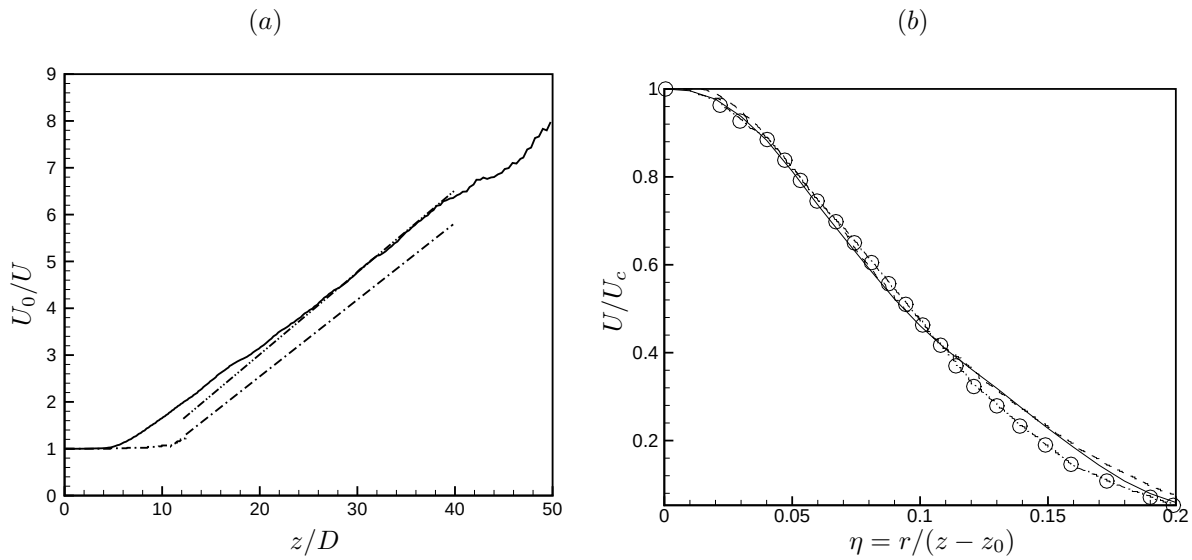

Figure 3. For turbulent jet at $Re = 2400$ (a): Mean axial velocity at jet centerline as a function of distance from jet exit plane (—··—) Wygnanski & Fiedler 1969, (—-—-—) Boersma et al 1998, (———) present DNS. (b): Comparison of mean axial velocity profile (———) in self–similarity coordinates with Hussein et al (- - - -), Panchapakesan & Lumley (—·—·—) and Boersma et al 1998 (○).

for entrainment from free–stream into jet near the jet exit plane. Accounting for entrainment near the jet exit effectively produces a co–flowing jet in the jet exit plane. The importance of accounting for such entrainment is discussed in more detail by Babu & Mahesh (2004). The domain extends $50D$ radially and $50D$ axially downstream of the jet exit. The unstructured capability of the solver helps to solve for the flow to large radial distances while keeping the grid size relatively low. The lateral boundaries have no–slip or wall boundary conditions, while a zero–gradient boundary condition is used at the outflow boundary. Note that this configuration resembles a nozzle placed in the center of a room as is typical of most experiments.

At the inflow, a top–hat velocity profile is used. The turbulent simulations were initialized with a pseudo–random velocity field of amplitude 0.1% of the jet exit velocity. Explicit time advancement with time step of $0.001D/U_0$ time units was used and the simulations were run for about $1200D/U_0$ to allow initial transients to exit the domain. Statistics were gathered over the next $1400D/U_0$ time units. The grid contains about 30 hexahedral elements in the radial span at the jet exit. Upto a distance of $10D$ are about 186 elements in the radial direction. From grid convergence studies, it was found that at an axial distance of $45D$, the jet grows to about $9D$ units radially. Therefore, beyond $10D$ the grid starts coarsening and at lateral domain, the elements are as big as $2D$ units. In the axial direction, the element size is about $0.06D$ near the jet exit. The elements grow as we go axially downstream and at an axial distance of $30D$, the axial resolution is about $0.2D$ units. At the exit domain, the elements are about $0.4D$. In the azimuthal direction, there are about 64 elements at the jet exit. At a radial distance of $10D$ from jet centerline, there are about 168 elements in the azimuthal direction and the elements start coarsening as we go radially toward the lateral domain. Near the lateral domain, there are about 160 elements. The unstructured capability helps in maintaining good resolution within the jet while maintaining the grid size relatively small by rapid coarsening in the free–stream. Since the topology of the domain is cylindrical, the radial and azimuthal resolution is same in the buffer region upstream to jet exit plane. In the axial direction, the resolution is about $0.4D$ units near the jet exit. This rapidly coarsens as we further move in the buffer region and at far upstream from jet exit plane, the element size in axial direction is about $1.8D$ units.

Convergence studies were performed on two different grids with varying grid resolution. Initially, the simulations were performed on a grid with 3.8 million hexahedral elements. The second set of simulations was performed on a grid with 6 million hexahedral elements. It was found that solutions like mean axial velocity and velocity fluctuations from both the domains agreed to plotting accuracy and therefore, the results from domain with 6 million elements are presented here. Independence from radial confinement effects (Hussein et al 1982, George 1990) was established by keeping the streamwise extent fixed and gradually varying the radial span. These tests were performed for a laminar jet at Reynolds number of 300 (Babu & Mahesh 2004) and the largest radial domain was used for the present computations.

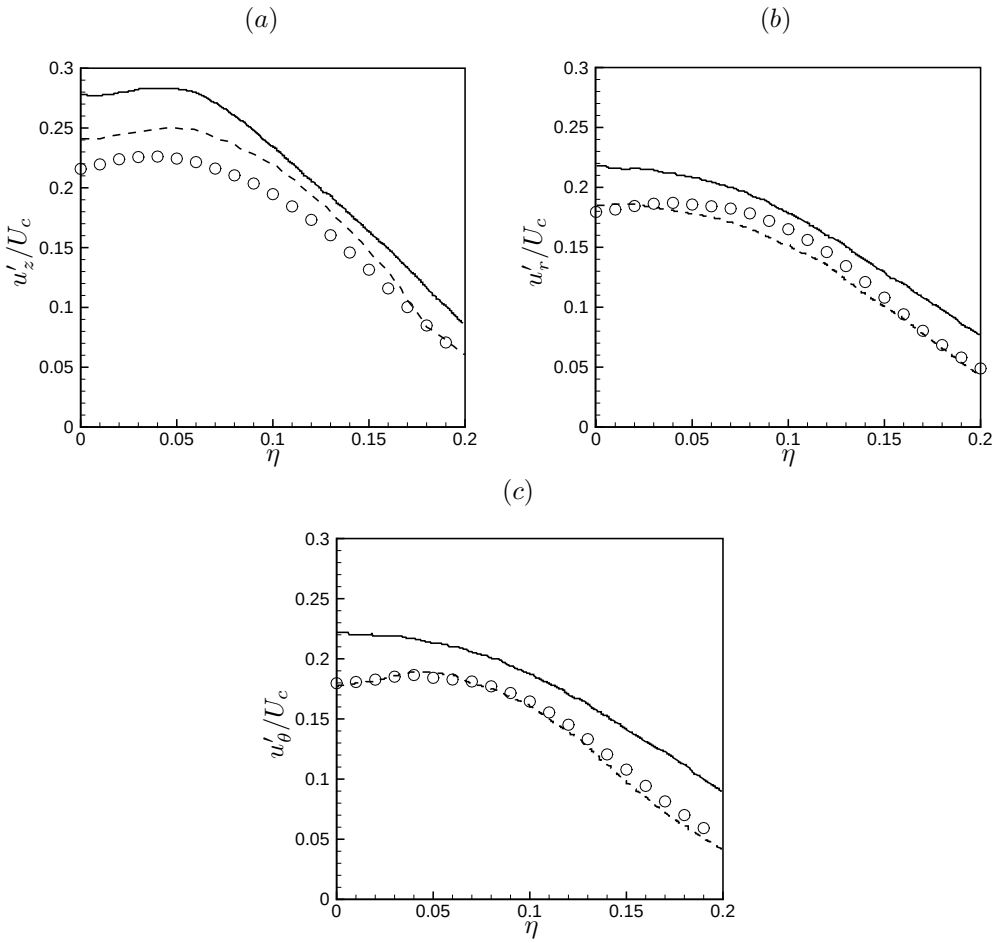

Figure 4. Comparison of DNS results to experiment. The turbulence r.m.s velocities scaled with local centerline velocity are plotted in similarity coordinates, $\eta = r/(z - z_0)$. (———) Hussein et al. (1994), (- - - -) Panchapakesan & Lumley (1993), (○) present DNS. (a): axial component, (b): radial component and (c): azimuthal component.

III. Results

A. Velocity field

The simulations are compared to the experimental data of Wygnanski & Fiedler (1969), Hussein et al (1994) and Panchapakesan & Lumley (1993), and numerical simulations of Boersma et al (1998). Wygnanski & Fiedler (1969) investigated axisymmetric incompressible turbulent isothermal jets using hot–wire anemometers. The jet had a laminar profile, and exited from a nozzle at Reynolds number of 10^5. They measured a variety of turbulent quantities e.g. mean velocity, turbulent stresses, intermittency, autocorrelation and skewness. Hussein et al (1994) performed experiments to estimate correlations for pressure–velocity and pressure–strain rate using laser Doppler measurements and stationary hot–wire for a round turbulent jet. These experiments were performed at a Reynolds number of 10^5 for a top–hat jet exhausting into a large room. Lubbers et al (2001) extended the simulations of Boersma et al (1998) by introducing a passive scalar in the flow. The conditions correspond to a jet issuing from an orifice in a wall. Stress–free lateral boundary conditions were used to facilitate entrainment from lateral boundaries. These simulations were performed at Reynolds number of 2000 and Schmidt number of 1. They conclude that while the profiles of mean concentration is self–similar in far field, the fluctuations are not self–similar. Figure 3a shows the centerline decay of mean axial velocity compared with experimental data of Wygnanski & Fiedler (1969) and a past numerical simulation by Boersma et al (1998). The main difference between the above two configurations is that, in the former experimental situation, the jet could entrain more near the jet exit from the domain upstream from the jet exit plane. Recall that the present simulations account for entrainment near jet exit through the buffer region.

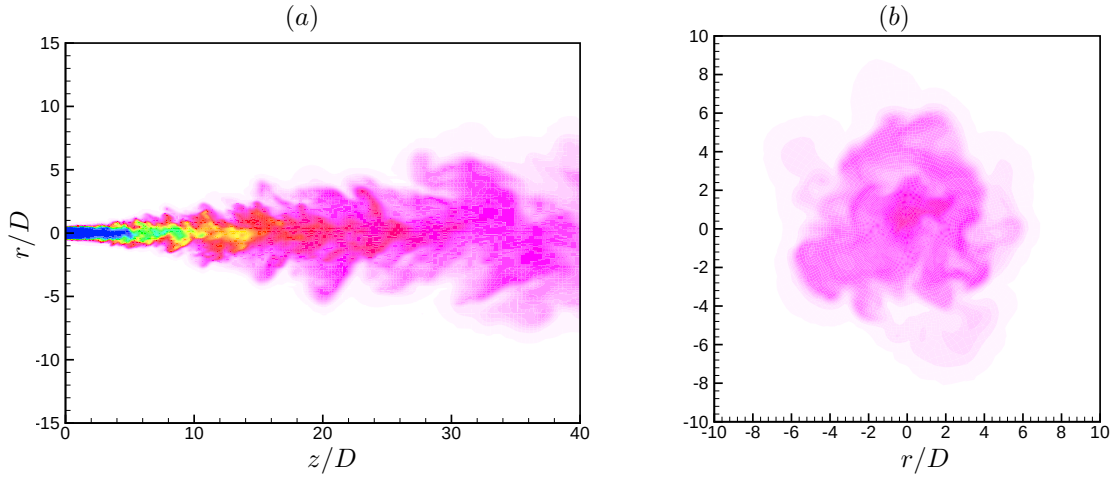

Figure 5. Contour plot of instantaneous scalar concentration. (a)**: Axial cross–section contour plot,** (b)**: Radial cross–section contour plot at axial location of** $Z/D = 30$**. Note: Only region closer to jet is shown for clarity.**

Figure 3a shows that the present simulations show good agreement with experimental data. The simulation data from Boersma et al (1998) shows the core closing around $10D$ while the present simulations show the core closing between $4D$–$5D$. Note that Boersma et al's (1998) focus was on the self–similar properties of the jet, which are unaffected by the longer potential core. Once the potential core closes and the jet attains self–similarity, the solutions plotted in self–similarity variables collapse for both the domains, with and without buffer region. Figure 3b shows the statistics of mean axial velocity profile normalized with the local centerline velocity plotted in self–similarity coordinates $\eta = r/(z - z_0)$. These self–similarity profiles are averaged through axial span of $15D$–$30D$. Good agreement with experiments is seen in figure 3b for mean axial velocity.

Figures 4a–c show the the three components of turbulent intensities plotted in similarity coordinates, $\eta = r/(z - z_0)$. The DNS is compared to curve–fits given by Hussein et al (1994) and Panchapakesan & Lumley (1993). The similarity profiles are obtained by averaging profiles over $15D \leq z \leq 40D$. Good agreement with Panchapakesan & Lumley (1993) is seen, particularly for the radial and azimuthal velocities. The axial intensities in figure 4a seem to be lower at the jet centerline. The two experimental results compared here were performed at a Reynolds number of about 10^5 and have top–hat velocity profiles at jet exit. Although the jet Reynolds number and exit velocity profiles are similar, appreciable variation in the self–similarity profiles is observed among experiments. George (1989, 1990) suggest that the governing equations allow similarity solutions which are very sensitive to factors like initial conditions and domain geometry. Note that the difference between present DNS results and experimental data from Panchapakesan & Lumley (1993) is less than the difference between the two experiments themselves.

B. Scalar field

The simulations were performed with a passive scalar with Schmidt number of 1. The passive scalar was introduced in the jet exit with a top–hat profile. Instantaneous contours of the passive scalar are shown in figure 5 where the wide range of scales of motion is apparent. Figure 6a shows the centerline decay of the mean scalar which is compared with experimental data varying with Reynolds number from $5000 - 16000$ and Schmidt number 0.7–800. In figure 6a, it is observed that the present DNS results have good agreement with the experimental results of Dahm & Dimotakis (1987) and Dowling & Dimotakis (1990). Both experiments were performed at a Reynolds number of 5000. The experiments by Dahm & Dimotakis (1987) were performed with a Schmidt number of 600–800 while the experiments of Dowling & Dimotakis (1990) were performed with a Schmidt number of 1. The comparison to experimental data is consistent with Dowling & Dimotakis (1990) who note that the mean concentration profile is independent of Schmidt number while the scalar fluctuations were found to depend on Schmidt number. The centerline scalar intensities are shown figure 6b. The present DNS results seem to be in good agreement with experimental results.

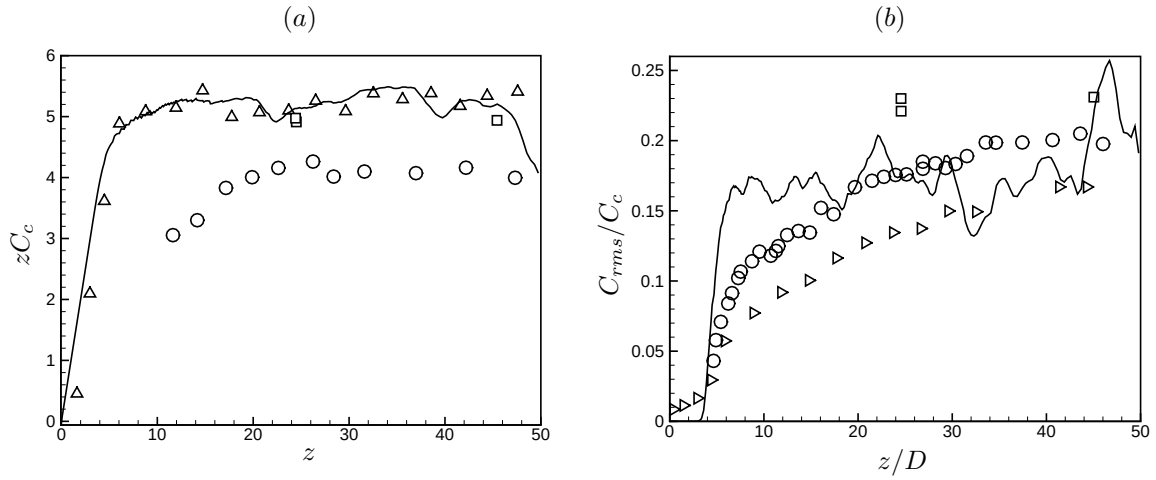

Figure 6. Centerline decay of passive scalar at $Re = 2400$ (a): Mean scalar scaled with distance from orifice center (b): rms of scalar fluctuations scaled with local mean scalar concentration. (———) DNS, (○) Birch et al. (1967) , (△) Dahm et al. (1987) and (□) Dowling & Dimotakis (1990).

IV. Phenomenology of scalar mixing

A. Instantaneous scalar profiles

It is well–known (e.g. Corrsin & Uberoi 1950, Becker et al 1967, Birch et al 1978, Lockwood & Moneib 1980, Dahm 1985 and Dowling & Dimotakis 1990) that the mean scalar profile is Gaussian. However past measurements (Uberoi & Singh 1975, Dahm & Dimotakis 1987, van Cruyningen al 1990) of instantaneous scalar profiles suggest that the instantaneous profiles of scalar differ considerably from Gaussian profiles; and appear 'top–hat' in nature. The obvious question is, 'how do instantaneous 'top–hat' profiles average to give a Gaussian mean?'. Schefer et al (1994) studied instantaneous scalar profiles in a non–reacting CH_4 turbulent jet at Reynolds number of 7000. They observed instantaneous scalar profiles that are different from mean Gaussian and suggested that the changes in profile shape could be due to entrainment caused by coherent motions at the outer edges of the jet.

The DNS data is used to study this behavior. Figures 7 a–c show the radial profiles of instantaneous axial velocity and scalar concentration normalized with their respective local centerline values at three different axial locations. The data in (———) corresponds to the instantaneous axial velocity while (- - - -) represents the passive scalar concentration. Shown in figure 7d is the contour plot of instantaneous scalar concentration with the corresponding streamlines. Three stations (A), (B) and (C) are chosen at three different axial locations along the jet axis. These stations are chosen such that entrainment from the free–stream into the jet increases as we move axially downstream. Figure 7a corresponds to axial station (A), figure 7b corresponds to axial station (B) and figure 7c corresponds to axial station (C). The radial profiles of the instantaneous axial velocity and scalar concentration in figure 7a corresponding to axial station (A) is seen to be qualitatively similar, and furthermore triangular instead of top–hat. At station (B), there is relatively more entrainment than station A into the jet by the coherent motions in positive radial direction as indicated by the streamlines. Figure 7b shows the radial profiles of instantaneous axial velocity and scalar concentration corresponding to the station (B) in figure 7d. It is observed that the instantaneous radial profiles are transitioning to a top–hat profile in the positive radial direction where there is relatively more entrainment into the jet. At station (C) the profile is almost 'top–hat' along both positive and negative radial planes. This correlates to the axial location where there is entrainment into jet along both the directions and that the passive scalar profile is uniform.

The conclusion therefore is that instantaneous profiles of both velocity and scalar are similar to each other. These instantaneous profiles are dictated by the large scale entrainment into the jet from the free–stream. Also, it has been observed that these profiles alternate between 'triangle' and 'top–hat' both spatially and temporally. The periodicity of this repetition of profiles along the jet flow is not clearly quantifiable due to insufficient domain length of $50D$ in the present simulations. These instantaneous profiles result in a Gaussian mean.

Van Cruyningen (1990) and Dimotakis et al (1983) report the presence of pure entrained fluid in the jet

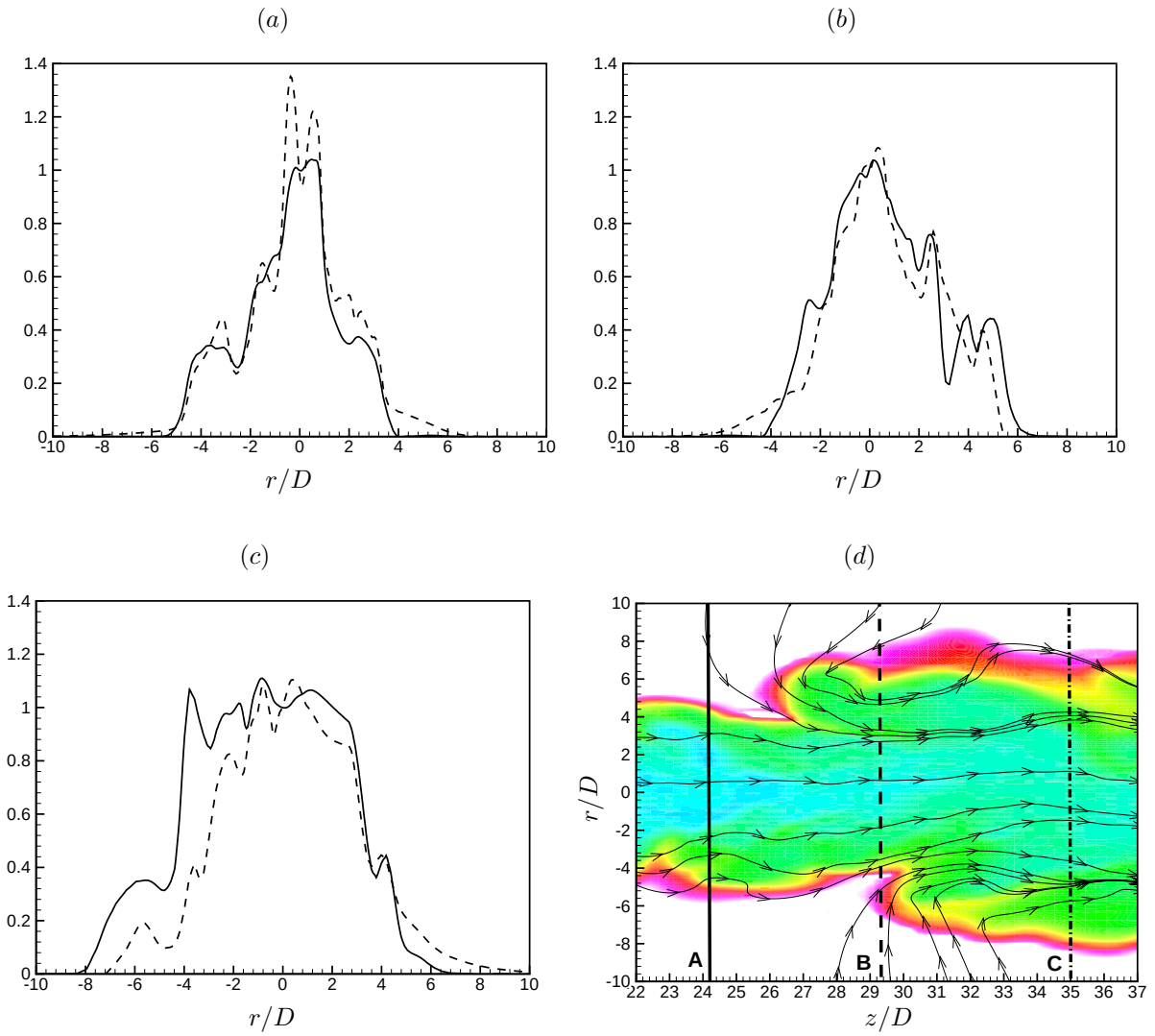

Figure 7. Comparison of instantaneous radial profiles of axial velocity (——) and passive scalar (- - - -) scaled with respective local centerline values at 3 different axial locations. (a): axial location of $26.0D$ corresponding before mixing, (b): axial location of $29.3D$ corresponding to mixing along positive radial axis, (c): axial location of $35.0D$ corresponding to complete mixing and (d): Instantaneous radial cross-section of scalar concentration contours shown closer to the jet to illustrate mixing. Note: stations A, B and C correspond to different axial stations in (a), (b) and (c).

centerline for water jets. The time history plots as shown in figure 7a–c, do not show that the instantaneous passive scalar concentration drops to zero at any instant of time. Recall that the Schmidt number in present simulations is 1 which is three orders of magnitude smaller than in water jets. The entrained scalar therefore diffuses more before it reaches the jet centerline. This behavior is consistent with the experiments of lower Schmidt number turbulent jets, e.g. Uberoi & Singh (1975, two–dimensional heated jet) and Schefer et al (1994, methane jet) where the instantaneous passive scalar concentration does not drop to zero at jet centerline.

B. The role of diffusion in scalar mixing

Viscous diffusion is central to two important aspects of scalar mixing. It determines scalar dissipation which is fundamental to flamelet models in turbulent combustion (Peters 1983). Viscous processes also determine the overall sensitivity of the jet to Reynolds and Schmidt numbers. In particular, as shown by Dimotakis (2000, figure 6 in his paper), jets undergo mixing transition at a certain Reynolds number beyond which scalar fluctuations at the jet centerline no longer depend on the Reynolds number. Experiments by Prasad & Sreenivasan (1990), Dowling & Dimotakis (1990), Su & Clemens (2003), and Buch & Dahm (1996, 1998)

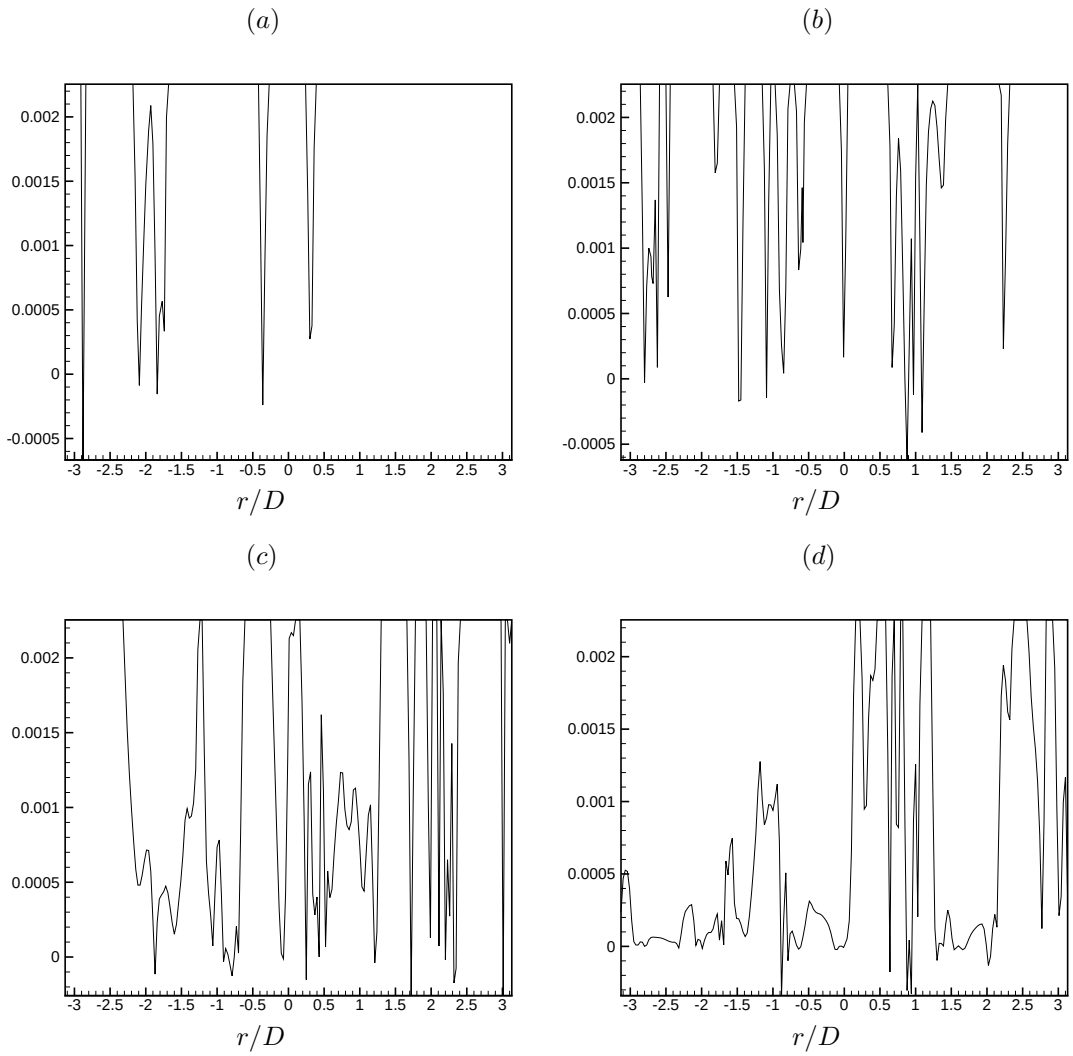

Figure 8. Instantaneous profiles of Ψ at four different radial locations as a function of jet azimuthal angle at axial location of $30Z/D$. (a): $r = 1D$, (b): $r = 2D$, (c): $r = 4D$ and (d): $r = 5D$. Note the increase in number of spikes toward 0 and the region encompassed within these spikes as r increases.

have studied scalar dissipation. Prasad & Sreenivasan (1990) performed quantitative three–dimensional measurements of passive scalar fields in a turbulent water jet using laser–induced fluorescence. Buch & Dahm performed experimental studies with higher Schmidt number ($Sc >> 1$, 1996) and lower Schmidt number ($Sc \sim 1$, 1998) to study self–similar distribution of dissipation layer thickness. The lower Schmidt number experiments were performed with propane as scalar and Reynolds number of $11000 - 14000$. High resolution two dimensional Rayleigh scattering images were taken in the far field self–similar regime of jet. They found that local dissipation layer thickness is related to outer scale as ${Re_\delta}^{-3/4}Sc^{-1/2}$ (Re_δ is defined as outer–scale Reynolds number). Also the largest and smaller layer thickness were found to follow the Kolmogorov scaling. Su & Clemens (2003) extended the work of Buch & Dahm for lower Schmidt number ($Sc \sim 1$) and Reynolds number of $3290 - 8330$ (based on outer–scales) by performing three–dimensional simultaneous planar Rayleigh scattering and planar laser–induced fluorescence. They study fine–scale scalar mixing by direct measurement of scalar dissipation structures and find that average thickness scales as ${Re_\delta}^{-3/4}Sc^{-1/2}$. These experimental data therefore suggest that scalar dissipation is concentrated in thin regions inside the jet – an observation that is central to 'flamelet' based models for turbulent combustion.

The Reynolds number dependence of scalar fluctuations in turbulent jets is summarized by Dimotakis 2000 (figure 6 of his paper) who shows normalized jet–fluid concentration variance at the centerline as a function of jet Reynolds number for liquid–phase and gas–phase jets. The data show that centerline scalar fluctuations for liquid–phase jets decreases with increasing Reynolds number and reaches an asymptotic value coinciding with that for gas–phase jets at sufficiently high Reynolds number (~ 10000).

These two aspects of the mixing process are studied by analyzing the diffusion and convection terms in

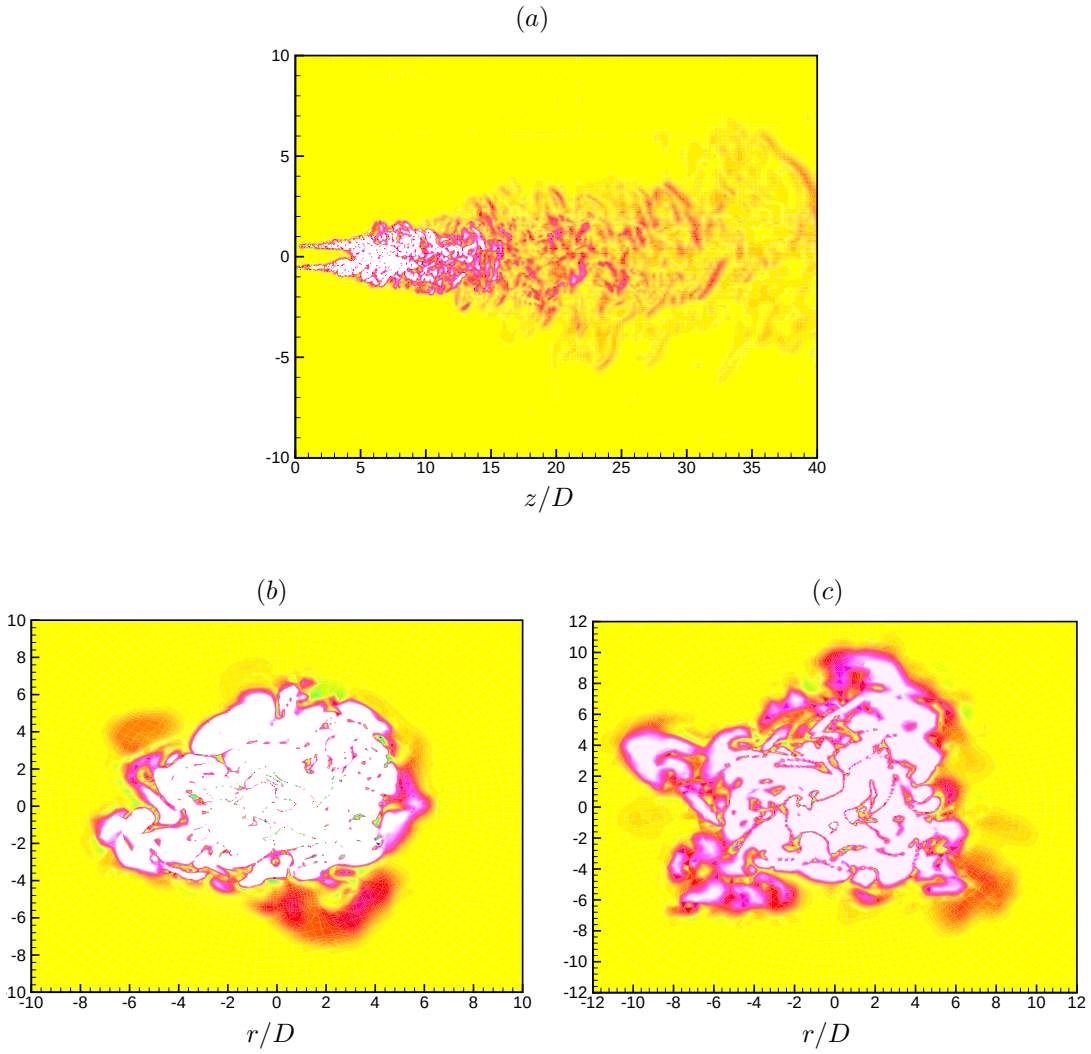

Figure 9. Instantaneous contour plots of Ψ. (a): Axial cross–section contour plot. (b): Radial cross–section contour plot at $Z/D = 30$ and (c): radial cross–section contour plot at $Z/D = 45$. Color scheme: white corresponds to convection important regions and blue corresponds to diffusion important regions. In figures (b) and (c) note the thin regions at jet center and 'brush' like near jet edge.

the passive scalar equation are analyzed (equations 4 & 5). A variable Ψ is introduced which is defined as the difference between convection and diffusion at any instant (equation 6).

$$Convective\ term : \frac{\partial(cu_i)}{\partial x_j} \tag{4}$$

$$Diffusive\ term : \frac{1}{Re\ Sc}\ \frac{\partial^2 c}{\partial x_j \partial x_j} \tag{5}$$

$$\Psi = (Convective\ term)\ -\ (Diffusive\ term) \tag{6}$$

Therefore, lower the value of Ψ, more important is contribution of diffusion to passive scalar transport at that given location at that instant of time. To perceive more clearly the regions where diffusion is important, the maximum value of Ψ in a axial cross–section plane is limited by the absolute minimum of Ψ in that plane as given by equation 7.

$$\Psi = (Convective\ term)\ -\ (Diffusive\ term)\ |\ max(\Psi) = \|min(\Psi)\|,\ \forall\ axial\ location \tag{7}$$

Figure 8a–c shows the variation of Ψ at an axial location of $30D$ from the orifice at different radii as a function of azimuthal angle. In figure 8a, it is observed that the regions where diffusion is important

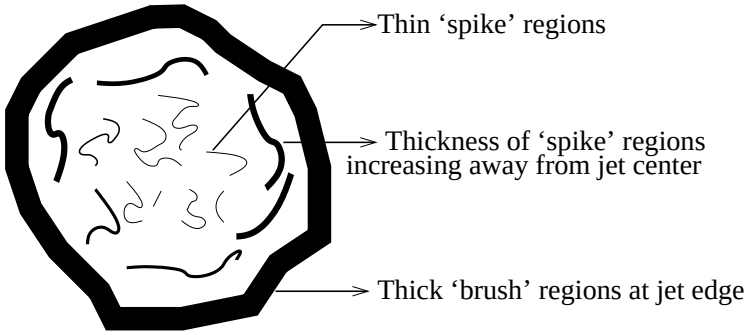

Figure 10. Schematic of radial cross–section showing diffusion important regions.

occurs in thin ‘spike’ regions closer to jet center which are very intermittent. As we go radially outward, the thickness of these ‘spike’ regions increases as shown in figure 8b–c. Toward the edge of the jet, the regions where diffusion is relatively more important encompasses almost the entire azimuthal angle as shown in figure 8d. Figure 9a shows an axial cross–section contour plot of Ψ. Figure 9b, c and d show the radial cross–section contour plots of Ψ at three different axial locations corresponding to $Z/D = 20$, $Z/D = 30$ and $Z/D = 45$ respectively. The trend of the diffusion dominated regions shown in plots 8a–c is observed clearly from the contour plots of radial cross–sections. At the jet edge, these diffusion important regions occur in thick ‘brush’ like regions which prevail through almost the entire azimuthal direction. This behavior is schematically shown in figure 10.

To quantify these regions where diffusion is relatively more important than convection, two variables Ω and Γ are introduced. Ω is defined as the thickness of these ‘spike–like’ regions and Γ is the area within these spike–like regions in figure 8a–d. Both Ω and Γ are averaged in time with using approximately 4000 samples. These averaged profiles are shown in figure 11a–b as a function of radial distance from jet center scaled with axial distance from jet orifice. These plots are shown for four different axial locations. From figure 11a it is seen that the thickness of the regions where diffusion is important, increases radially from the jet centerline and reaches a maximum toward the jet edge. At the jet edge, it is seen that Ω is almost 2π indicating diffusion important regions spans almost the entire azimuthal angle. Figure 11b shows the contribution of these diffusion important regions as a function of radial distance, similar to the Ω plot. It is seen that these diffusion important regions gain importance with increasing radial distance and contributes the maximum toward the edge of the jet.

The thickness of the regions where diffusion is important, is explained as follows. Let l_{conv} and l_{diff} denote the length scales of convection and diffusion respectively in the jet. u_{conv} represents the average convective velocity at a radial cross–section of jet. In the regions where diffusion is comparable to convection, the terms in equations 4 and 5 should be comparable. This leads to

$$\frac{c\ u_{conv}}{l_{conv}} \sim \frac{1}{Re\ Sc}\ \frac{c}{l_{diff}^2} \tag{8}$$

Simplifying and rearranging the terms,

$$l_{diff} \sim \sqrt{\frac{1}{Re\ Sc}\ \frac{l_{conv}}{u_{conv}}} \tag{9}$$

Equation 9 shows that the length scale of the regions where diffusion is important depends on the Reynolds number, Schmidt number, convective length scales and convective velocity. For a given Reynolds number and Schmidt number, the diffusion length scale varies as square root of convective time scale (l_{conv}/u_{conv}). At a given axial location, the convective length scales are expected to increase from the jet center toward the jet edge, where there is entrainment by large structures from free–stream into the jet. Also the convective velocity can be assumed to scale with the rms level of the velocity fluctuations. These velocity fluctuations decrease (Figure 4a–c) from the jet center and is about 0.05 times centerline mean velocity at jet edge. This implies that the convective time scale (ratio of convective length scale to velocity) increases from jet center

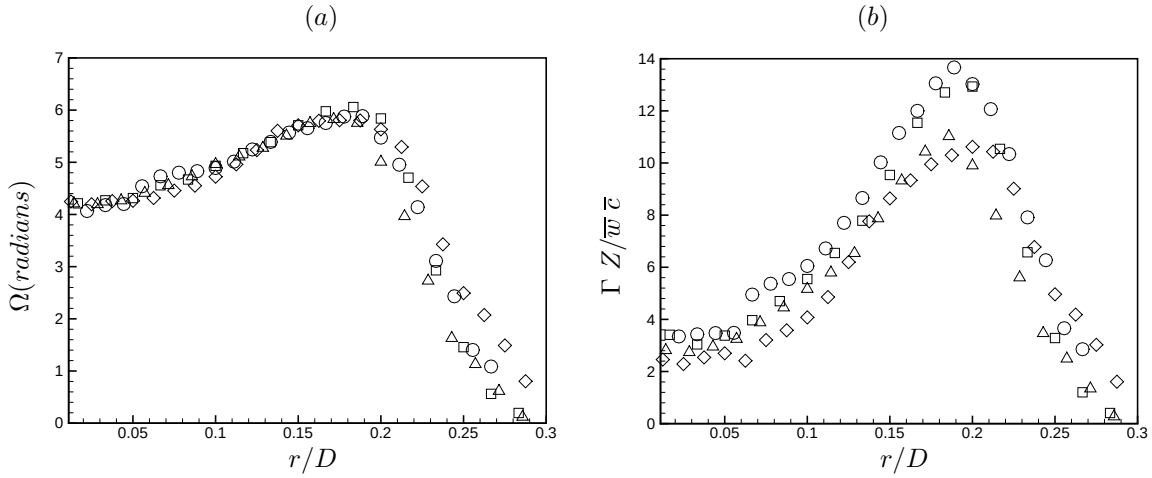

Figure 11. For Re=2400 turbulent jet, (a): radial profiles of diffusion important regions i.e., Ω at various axial locations as a function of radial distance non–dimensionalized with axial distance from jet exit plane (b): radial profiles showing contribution of diffusion important regions i.e., Γ non–dimensionalized with axial distance from jet exit plane, mean axial velocity at jet centerline and mean scalar concentration at jet centerline. (□) $Z = 30D$, (△) $Z = 35D$, (◇) $Z = 40D$ and (○) $Z = 45D$.

to reach maximum at the jet edge. Equation 9 therefore suggests that the diffusion length scale increases toward the outer edge of the jet. The increased residence time for fluid near the edge of jet causes diffusive processes to be important near the edge of jet.

Equation 9 shows the dependence of diffusion length scales on Reynolds number and Schmidt number. With increasing Reynolds number and/or Schmidt number, the thickness of the regions where diffusion is important decreases, which implies that the thickness of these 'brush' regions near the jet edge decreases. At sufficiently high Reynolds numbers, the thickness of these 'brush–like' regions becomes very small relative to width of the jet. It is speculated that the scalar fluctuations undergo mixing transition once these outer regions are thin compared to the jet diameter, and further increases in Reynolds number do not yield noticeable changes in the scalar intensities.

V. Summary

Direct numerical simulation of a spatially evolving turbulent jet is performed at Reynolds number of 2400. An inflow buffer region is provided upstream of the jet exit plane to account for entrainment near inflow. A passive scalar of Schmidt number 1 is introduced at the jet exit. The instantaneous radial profiles of velocity and passive scalar are shown to be similar to each other and that they alternate between 'top–hat' and 'triangle' profiles, both spatially and temporally. The profiles are found to be dictated qualitatively by the entrainment from free–stream into jet. This instantaneous behavior results in a mean Gaussian profile. The instantaneous convective and diffusive terms in passive scalar transport equation are analyzed and diffusive dominated regions are studied. Diffusion dominated regions occur in thin regions closer to the jet center and thick 'brush–like' regions near the jet edge. The width of these brush–like regions are suggested to decrease with increase in Reynolds number. It is speculated that mixing transition occurs when the Reynolds number is high enough that these outer brush–like regions are thin compared to the jet width.

Acknowledgments

We are grateful to the Department of Energy for their financial support through the Stanford ASCI Alliance Program. Computing time was provided by the Minnesota Supercomputing Institute, San Diego Supercomputer Center and National Center for Supercomputing Applications.

References

[1]Batchelor, G. K. 1959, Small scale variation of convected quantities like temperature in turbulent fluid, *J. Fluid Mech.*, **5:** 113–139.

[2]Becker, H. A., Hottel, H. C. & Williams, G. C. 1967, The nozzle fluid concentration field of the round turbulent jet, *J. Fluid Mech.*, **30:** 285–303.

[3]Buch, K. A. & Dahm, W. J. A. 1996, Experimental study of the fine-scale structure of conserved scalar mixing in turbulent flows. Part 1. Sc 1, *J. of Fluid Mech.*, **317:** 21–71.

[4]Buch, K. A. & Dahm, W. J. A. 1998, Experimental study of the fine-scale structure of conserved scalar mixing in turbulent flows. Part 2. Sc = 1, *J. of Fluid Mech.*, **364:** 1–29.

[5]Birch, A. D., Brown, D. R., Dodson, M. D. and Thomas, J. R. T. 1978, The turbulent concentration field of a methane jet, *J. Fluid Mech.*, **88:** 431–449.

[6]Boersma, B. J., Brethouwer, G. & Nieuwstadt, F. T. M. 1998, A numerical investigation on the effect of the inflow conditions on the self-similar region of a round jet, *Phys. Fluids*, **10(4):** 899–909.

[7]Breidenthal, R. E. 1981, Structure in turbulent mixing layers and wakes using a chemical reaction, *J. Fluid Mech.*, **109:** 1–24.

[8]Broadwell, J. E. & Breidenthal, R. E. 1982, A simple model of mixing and chemical reaction in a turbulent shear layer, *J. Fluid Mech.*, **125:** 397–410.

[9]Broadwell, J. E. & Mungal, M. G. 1991, Large–scale structures and molecular mixing, *Phys. Fluids*, **3(5):**1193–1206

[10]Corrsin, S. 1943, Investigation of flow in an axially symmetrical heated jet of air, *NACA, Wash. Wartime Report*, W-94.

[11]Corrsin, S. 1951, On the spectrum of isotropic temperature fluctuations in isotropic turbulence, *J. Appl. Phys.*, **22:** 469–473.

[12]Corrsin, S. & Uberoi, M. S. 1950, Further experiments on the flow and heat transfer in a heated turbulent air jet, *NACA Rep.*, 998.

[13]Corrsin, S. & Uberoi, M. S. 1951, Spectra and diffusion in a round turbulent jet, *NACA Rep*, 1940.

[14]Dahm, W. J. A. 1985, Experiments on entrainment, mixing and chemical reactions in turbulent jets at high Schmidt number. Ph.D, thesis, California Institute of Technology, Pasadena, CA.

[15]Dahm, W. J. A., & Dimotakis, P. E. 1985, Measurements of Entrainment and Mixing in Turbulent Jets," *AIAA 23rd Aerospace Sciences Meeting*, Paper 85-0056.

[16]Dahm, W. J. A. & Dimotakis, P. E. 1987, Measurements of entrainment and mixing in turbulent jets, *AIAA J.*, **25:** 1216–1223.

[17]Dimotakis, P. E. 2000, Mixing transition in turbulent flows, *J. Fluid Mech.*, **409:** 69–98.

[18]Dowling, D. R. and Dimotakis, P. E. 1990, Similarity of the concentration field of gas–phase turbulent jets, *J. Fluid Mech.*, **218:** 109–141.

[19]George, W. K. 1989, The self–preservation of turbulent flows and its relation to initial conditions and coherent structures, *Advance in Turbulence (ed. George, W. K. & Arndt, R. E. A)*, 39–72.

[20]George, W. K. 1990, Governing equations, experiments and the experimentalist, *Expl. Thermal Fluid Sci.*, **3:** 557-566.

[21]Hussein, H. J., Capp, S. P, & George, W. K. 1994, Velocity measurements in a high Reynolds number, momentum-conserving axisymmetric turbulent jet, *J. Fluid Mech.*, **258:** 31–75.

[22]Kerstein, A. R. 1990, Linear–eddy modeling of turbulent transport, Part 3. Mixing and differential molecular diffusion in round jets, *J. Fluid Mech.*, **216:** 411–435.

[23]Lockwood, F. C. & Moneib, H. A. 1980, Fluctuating temperature measurements in a heated round free jet, *Combust. Sci. Tech*, **22:** 63–81.

[24]Lubbers, C. L., Brethouwer, G. & Boersma, B. J. 2001, Simulation of the mixing of a passive scalar in a round turbulent jet, *Fluid Dynamics Research*, **28:** 189–208.

[25]Mahesh, K., Constantinescu, G. & Moin, P. 2004, A numerical method for large–eddy simulation in complex geometries, *J. Comp. Phys.*, **197:** 215–240.

[26]Oboukhov, A. M. 1949 Structure of the temperature field in turbulent flows, *Izv. Ak. Nauk SSR, Geogr. Geophys.*, **13:** 58–69.

[27]Panchapakesan, N. R. & Lumley, J. L. 1993, Turbulence measurements in axisymmetric jets of air and helium. Part 1. Air jet, *J. Fluid Mech.*, **246:** 197–223.

[28]Pantano, C., Sarkar, S. & Williams, F. A. 2003, Mixing of a conserved scalar in a turbulent reacting shear layer, *J. Fluid Mech.*, **481:** 291–328.

[29]Peters, N. 1983, Local quenching due to flame stretch and non-premixed turbulent combustion, *Combust. Sci. Tech.*, **30:** 1–17.

[30]Prasad, R. R. & Sreenivasan, K. R. 1990, Quantitative three–dimensional imaging and the structure of passive scalar fields in fully turbulent flows, *J. Fluid Mech.*, **216:** 1–34.

[31]Schefer, R. W., Kerstein, A. R., Namazian, M. & Kelly, J. 1994, Role of large–scale structure in a non–reacting turbulent CH_4 jet, *Phys. Fluids*, **6(2):** 652–661.

[32]Lester, K. S. and Clemens, N. T. 2003, The structure of fine–scale scalar mixing in gas–phase planar turbulent jets, *J. Fluid Mech.*, **488:** 1–29.

[33]Uberoi, M. S. and Singh, P. I. 1975, Turbulent mixing in a two-dimensional jet, *Phys. Fluids*, **18:** 764.

[34]van Cruyningen, I., Lomno, A. & Hanson, R. K. 1990, Quantitative imaging of concentration by planar laser–induced fluorescence, *J. Exp. Fluids*, **10:** 41.

[35]Warhaft, Z. 2000, Passive scalars in turbulent flows, *Ann. Rev. Fluid Mech.*, **32:** 203–240.

[36]Wygnanski, I & Fiedler, H. E, 1969, Some measurements in the self preserving jet, *J. Fluid Mech.*, **38:** 577–612.